Zhang *et al. Microstructures* 2024;4:2024039
**DOI:** 10.20517/microstructures.2023.99

**Microstructures**

**Research Article**

**Open Access**

Check for updates

# Direct visualization of spin-dependent orbital geometry on the $Na_2IrO_3$ surface with ultra-high resolution

**Xin Zhang[1,#], Zongyuan Zhang[2,#], Jasminka Terzic[3,#], Zhibin Shao[1], Haigen Sun[4], Shaojian Li[4], Krisztián Palotás[5,6], Haoxuan Ding[7], Gang Cao[3], Wenliang Zhu[1], Haiping Lin[1], Jianzhi Gao[1], Minghu Pan[1,4]**

[1]School of Physics and Information Technology, Shaanxi Normal University, Xi'an 710119, Shannxi, China.
[2]Information Materials and Intelligent Sensing Laboratory of Anhui Province, Institutes of Physical Science and Information Technology, Anhui University, Hefei 230601, Anhui, China.
[3]Department of Physics, University of Colorado at Boulder, Boulder, CO 80309, USA.
[4]School of Physics, Huazhong University of Science and Technology, Wuhan 430074, Hubei, China.
[5]Wigner Research Center for Physics, Budapest H-1525, Hungary.
[6]MTA-SZTE Reaction Kinetics and Surface Chemistry Research Group, University of Szeged, Szeged H-6720, Hungary.
[7]School of Physics and Astronomy, University of Birmingham, Birmingham B15 2TT, UK.
[#]Authors contributed equally.

**Correspondence to:** Prof./Dr. Gang Cao, Department of Physics, University of Colorado at Boulder, G223 and G318, Boulder, CO 80309, USA. E-mail: gang.cao@colorado.edu; Prof./Dr. Minghu Pan, School of Physics and Information Technology, Shaanxi Normal University, 620 West Chang'an Street, Chang'an District, Xi'an 710119, Shannxi, China. E-mail: minghupan@hust.edu.cn; Prof./Dr. Jianzhi Gao, School of Physics and Information Technology, Shaanxi Normal University, 620 West Chang'an Street, Chang'an District, Xi'an 710119, Shannxi, China. E-mail: jianzhigao@snnu.edu.cn

**How to cite this article:** Zhang X, Zhang Z, Terzic J, Shao Z, Sun H, Li S, Palotás K, Ding H, Cao G, Zhu W, Lin H, Gao J, Pan M. Direct visualization of spin-dependent orbital geometry on the $Na_2IrO_3$ surface with ultra-high resolution. *Microstructures* 2024;4:2024039. https://dx.doi.org/10.20517/microstructures.2023.99

**Received:** 25 Dec 2023 **First Decision:** 15 Mar 2024 **Revised:** 27 Mar 2024 **Accepted:** 22 Apr 2024 **Published:** 27 Jun 2024

**Academic Editor:** Yi Du **Copy Editor:** Fangyuan Liu **Production Editor:** Fangyuan Liu

## Abstract

The honeycomb iridate $Na_2IrO_3$, as a candidate for the Kitaev model, has drawn increasing attention in recent years. It is a rare example of a strongly correlated, topologically nontrivial band structure that may have protected quantum spin Hall states. The nature of its intriguing insulating phase and magnetic order is still under debate. In the present work, we combine low-temperature scanning tunneling microscopy/spectroscopy and density functional theory calculations to show that $Na_2IrO_3$ exhibits a band gap of 420 meV at 77 K, indicating a novel relativistic Mott insulator rather than Slater-like states. In addition, it is demonstrated that the Ir-O-Ir bonds and the subtle local density of states variation of Ir atoms induced by spin correlations can be imaged in real space in ultra-high resolution utilizing a spin-polarized oxygen-functionalized scanning tunneling microscopy tip. The direct

observation of the zigzag Ir-O-Ir bonds at 77 K strongly dictates the zigzag magnetic ordering below $T_N \approx 15$ K because of the strong spin-orbit interactions that lock the lattice and magnetic moments.

**Keywords:** Iridate, scanning tunneling microscopy, strong-correlated materials, high-resolution imaging, spin-correlation

## INTRODUCTION

The $A_2IrO_3$ ($A$ = Na, Li, *etc.*) honeycomb iridate is among the most debated iridate compounds, with the $Na_2IrO_3$ being especially interesting. A Kitaev-Heisenberg (KH) magnetic ground state[1-3] and a quantum spin liquid (QSL) phase[4-6] have been proposed in this compound. This material is expected to possess a topologically nontrivial band structure with protected metallic surface states[7-9]. Specifically, a quantum spin Hall (QSH) state has been predicted in the stacked 3D configuration of $Na_2IrO_3$[7,8]. Experimental studies have suggested that $Na_2IrO_3$ is a relativistic Mott insulator[10-12]. However, another study indicated that it is a Slater insulator[13]. The subsequent discovery of the zigzag-type magnetic order[3,4,14] also challenges the KH model. So far, numerous modifications of this model have been proposed[15-17], accompanied with extensive experimental efforts to adjust the relevant materials to the QSL ground state near the Kitaev limit[18-22]. Despite the partial success of the previous investigations, supporting experimental evidence remains lacking for the presence of the Kitaev ground state, spin liquid phase and the topologically nontrivial band structure in the $Na_2IrO_3$ compound. Such contradiction may imply that the band topology of $Na_2IrO_3$ is sensitive to the details of orbital geometry. Consequently, small variations of the structure or the interaction strength could lead to a quantum phase transition, e.g., the change of its topological characteristics[8,23-26]. On the other hand, the spin structure in correlated oxides plays an essential role in determining their physical properties due to the strong interplay between charge, orbitals and spins of transition metal oxides (TMOs)[6]. Consequently, the experimental approach that simultaneously provides information on the structures, orbitals and spins of this correlated material is highly desirable.

Scanning tunneling microscopy/spectroscopy (STM/S) are powerful tools with high spatial and energy resolutions. In particular, great success has been achieved in their applications in the study of high-$T_c$ superconducting cuprates[27]. Despite that, the atomic-resolved STM imaging on the surfaces of complex oxides remains very challenging due to the insulating nature of the materials and the strong interactions between samples and STM tips[10,28]. Usually, the density of states (DOS) of the oxygen anions and the related orbitals of cationic transition metals can hardly be resolved in the topographic STM images. Furthermore, spin-polarized STM imaging has been successfully achieved on the surface of magnetic metals by antiferromagnetic $CrO_2$ tips[29-31] and spin-polarized magnetic-coated tips[32-35]. Spin-polarized imaging on the surfaces of complex oxides has rarely been obtained.

This work reports that ultra-high resolution STM imaging can be achieved on the $Na_2IrO_3$ surface using an oxygen-functionalized STM tip. A Mott-type gap is observed in the tunneling spectroscopy at a temperature far above the transition temperature of the antiferromagnetic order of $Na_2IrO_3$, and such a gap has a downshift of the Fermi energy at the sites of oxygen vacancies. Orbital geometry of the Ir-O-Ir bonds and the subtle local DOS variation of Ir atoms induced by spin correlations are visualized directly in the topographic STM images due to the strong spin-orbit coupling (SOC), which provides a direct evidence for the zigzag magnetic ordering in this material.

## MATERIALS AND METHODS

### STM

The crystals used in this study have the typical sizes of 2 mm × 2 mm × 0.5 mm. Samples were cleaved *in situ* at room temperature (RT) under vacuum with pressure better than $1 \times 10^{-10}$ torr. The cleaved sample was quickly transferred into a Unisoko-1300 commercial STM for measurement at a temperature of 77 K. A commercial Pt-Ir tip was prepared by gentle field emission above a clean Au(111) sample. The bias voltage was applied on the sample during the STM observations. The STM images were analyzed using WSxM, a freeware scanning probe microscopy software based on Microsoft Windows[36].

### Calculation

The first-principles density functional theory (DFT) calculations were carried out with the Vienna Ab Initio Simulation Package (VASP)[37]. The core and valence electronic interactions were described with the frozen-core projector augmented-wave (PAW) potentials[38]. The Kohn-Sham single electron states were expanded in plane waves with an energy cut-off of kinetic energy of up to 400 eV. The exchange-correlation energy was calculated with the Perdew-Burke-Ernzerhof (PBE) of generalized gradient approximation (GGA)[39]. The tolerance of $10^{-4}$ eV was chosen for energy convergence of electronic calculations. The $Na_2IrO_3$ was modeled with a (2 × 2) unit cell. The metal STM tip was modeled with a pyramid of Ir(111) in which the apex is a single Ir atom. The oxygen-functionalized tip was mimicked by an Ir(111) pyramid with five oxygen atoms at the apex. A large vacuum of 25 Å along the direction normal to the surface was employed to separate surfaces from their periodic images. The Brillouin zone of reciprocal space was modeled based on the Γ centered Monkhorst-Pack scheme, where a 4 × 2 × 1 grid was used in geometry optimizations and calculations of electronic properties. STM images were simulated using the revised Chen method implemented in the bSKAN code[40].

## RESULTS AND DISCUSSION

### STM characterization of the sample surface

A representative topographic STM image at positive bias voltage ($V_b$ = +1.5 V) for the cleaved $Na_2IrO_3$ surface is shown in Figure 1A. The honeycomb lattice is clearly resolved. The measured lattice distance is about 5.2 Å, close to the distance between nearest neighbor Na atoms in the $NaIr_2O_6$ slab (about 5.3 Å)[10,14]. It has been reported that the empty-state STM images on oxide surfaces usually visualize the cationic atoms, e.g., Sr atoms in ruthenates and Ti atoms in $TiO_2$ (110) surfaces[41,42]. On this surface, sodium atoms buckle about 1.59 Å higher than the Ir-O plane in the optimized surface structure of $Na_2IrO_3$, as shown in Supplementary Figure 1. We, therefore, assign the observed honeycomb lattice to the array of the sodium atoms in the exposed $NaIr_2O_6$ layer. Each Na atom is surrounded by six edge-shared $IrO_6$ octahedra, as indicated by the inset of Figure 1A. The STM observations are consistent with the 1 × 1 arrangement of Na atoms in the $NaIr_2O_6$ slab, as reported previously[43]. Moreover, two types of defects ($\alpha$ and $\beta$) are identified at the atomic scale on the surface. As shown in Figure 1B, defect $\alpha$ appears as a dark hole in both the empty and filled-states images. Considering that it is located at the sodium position, we assign it to the Na vacancy. Defect $\beta$ is imaged as a bright protrusion at positive biases [Figure 1A] and as a dark pinhole surrounded by adjacent bright spots at negative biases [Figure 1B]. We assign it to the oxygen vacancy. Such assignments are confirmed by the STM simulations. As shown in Figure 1B, the simulated images for both the proposed Na and O vacancies agree well with the STM observations. In addition, the STS spectra [Figure 1C] taken at the pristine $Na_2IrO_3$ surface (red) and the site of defect $\beta$ (black) are compared. Both spectra exhibit a fully opened band gap near the Fermi level with a gap width of about 420 meV. The d$I$/d$V$ spectrum of defect $\beta$ has a 0.22 eV downshift of the Fermi energy, implying electron-type doping.

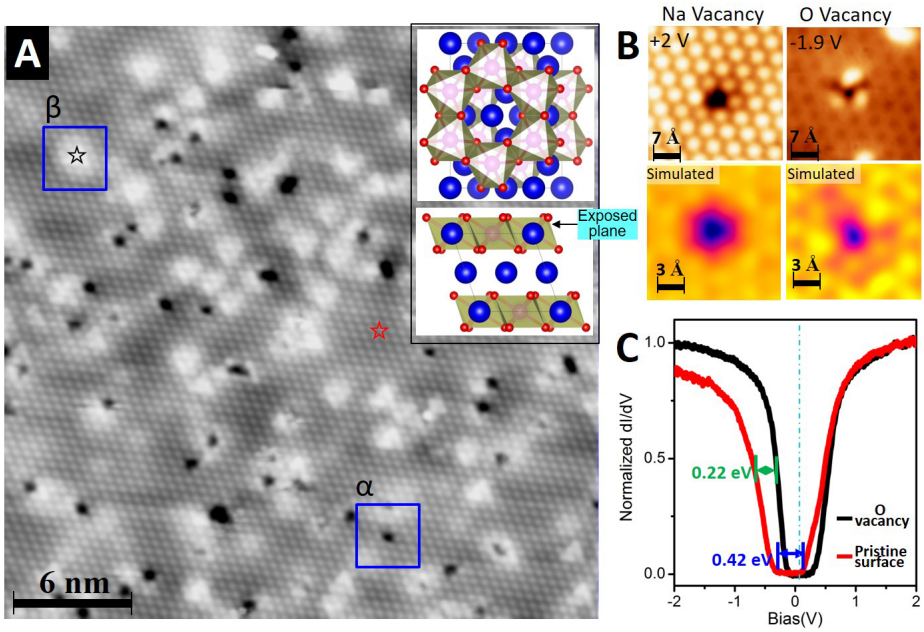


**Figure 1.** STM topographic images and the tunneling spectrum of the cleaved $Na_2IrO_3$ surface. (A) The representative STM topographic image of the RT-cleaved surface of $Na_2IrO_3$ ($V_b$ = +1.5 V, $I_t$ = 20 pA, image size: 30 × 30 $nm^2$). The inset shows the corresponding crystalline structure of $Na_2IrO_3$. The Na, O and Ir atoms are represented with blue, red and pink balls, respectively. (B) The upper panel shows the highly resolved STM images of two types of surface defects, assigned as Na and O vacancies, respectively. The corresponding simulated images of Na and O vacancies are provided in the lower panel, and their bias voltages are $V_b$ = +2.0 and -1.9 V, respectively. (C) *dI/dV* curves measured at the pristine surface and the site of the O vacancy, respectively ($T$ = 77 K). Both spectra possess a uniform fully opened gap. The gap width is 420 meV. STS spectra were acquired using a lock-in technique with *AC* modulation of 15 mV.

The tunneling spectra have been acquired over hundreds of times at different locations on the surface, producing essentially very similar gap features. It is worth noting that the spectra with a *U*-shape gap were measured at 77 K, far above the transition temperature of the antiferromagnetic order of $Na_2IrO_3$ ($T_N \approx 15$ K)[2,10]. Therefore, this observation may effectively exclude the possibility of a Slater-like state. Consequently, our spectroscopic analysis helps answer one of the long-term debated issues about this material, that is, whether $Na_2IrO_3$ is a relativistic Mott insulator[10-12] or a Slater insulator[13]. The major difference between Mott and Slater insulators depends on the role of magnetic interactions in gap formation, where Coulomb and exchange interactions drive gap formation in a Mott-Hubbard insulator, Coulomb interactions alone drive gap formation in a Mott insulator, while magnetic ordering drives gap formation in a Slater insulator. For example, a $J_{eff}$ = 1/2 Mott-Hubbard scenario has been suggested for the layered 5d TMO, $Sr_2IrO_4$ from angle-resolved photoemission spectroscopy (ARPES)[44] and resonant X-ray scattering (RXS)[45] measurements. A Slater mechanism has been found in other 5d TMOs such as $NaOsO_3$[46], where the Slater transition is demonstrated unambiguously by showing the coincidence of the metal-insulator transition (MIT) and the onset of long-range commensurate magnetic order based on the results of neutron and X-ray scattering. The interplay between on-site Coulomb repulsion (U), bandwidth (W) and SOC in 5d correlated electronic systems gives rise to a broad spectrum of novel phenomena; e.g., MIT may switch from Mott type to Slater type[47]. The observed gap width (420 meV) is reasonable by comparing with that obtained by ARPES (340 meV)[11]. According to the previous ARPES results[11], the maximum of the first-occupied Ir 5*d*-$t_{2g}$ band appears at -0.5 eV, agreeing well with the fact that the left rising edge of the DOS gap appears near -0.5 V in our d*I*/d*V* spectrum [Figure 1C]. The gap of 420 meV corresponds to the on-site Coulomb repulsion *U* between $J_{eff}$ = 1/2 bands. It is now recognized that the SOC is approximately 0.4 eV in the iridates, and rigorously competes with the on-site Coulomb repulsion *U*

(0.4~2.5 eV), which is significantly reduced because of the extended nature of the 5*d* orbitals[14,44]. Furthermore, after annealing the sample at 573 K for 5 min, we found that about two-thirds of the surface Na atoms are desorbed and the surface unit cell transforms from 1 × 1 to $(\sqrt{3} \times \sqrt{3})R30°$ [Supplementary Figure 2]. Accompanying this structural change, the insulating gap reduces from 420 to 300 meV, with a small shift of the gap feature in the spectra, illustrating the electron doping effect possibly due to the creation of extra oxygen vacancies during the annealing and the bandwidth broadening induced by electron doping [Supplementary Figure 3].

### DFT calculated PDOS and simulated STM images

The electronic structure of $Na_2IrO_3$ was revealed by DFT calculations. The optimized surface structure of $Na_2IrO_3$ is shown in Supplementary Figure 3. The relaxed structural parameters, such as the O-Ir-O bond lengths and the bond angles, agree well with previous X-ray diffraction measurements[10,14], implying that the surface $IrO_6$ octahedra are essentially the same as in the bulk except that surface Na atoms buckle 1.59 Å out of the Ir-O plane. The projected DOS (PDOS) for each species of atoms calculated by considering the SOC is shown in Figure 2A. As seen, the total DOS is mostly contributed by the iridium and oxygen atoms. According to previous theoretical[9] and experimental[11] discussions, the Ir 5*d* states are split into $t_{2g}$ and $e_g$ orbital states by the crystal field. As the SOC has been considered, the $t_{2g}$ band further splits into $J_{eff}$ = 1/2 doublet and $J_{eff}$ = 3/2 quartet bands. With the $J_{eff}$ = 3/2 band filled and having one remaining electron, the system is effectively reduced to a half-filled $J_{eff}$ = 1/2 single band system (schematic shown in Inset of Figure 2A). The $J_{eff}$ = 1/2 spin-orbit integrated states form a narrow band so that even small $U$ opens a Mott gap, making it a $J_{eff}$ = 1/2 Mott insulator. A prominent gap of about 0.4 eV width is clearly visible in the calculated DOS, agreeing well with both our STS measurement [Figure 1C] and the previously reported ARPES data[11]. It is worth noting that our calculations are consistent with those reported previously[7], where the DOS peaks correspond to the Ir 5*d*-$t_{2g}$ ($J_{eff}$ = 3/2 and $J_{eff}$ = 1/2) bands, respectively. The simulated STM images for the pristine honeycomb lattice of $Na_2IrO_3$ surface are shown in Figure 2B. An excellent agreement can be seen between the theoretical calculations and experimental observations [Figure 2B and C] at both positive and negative bias voltages. In the optimized slab model, the top layer of sodium atoms moves up by about 1.59 Å from their bulk crystal positions [Supplementary Figure 3] upon structural relaxation, and they are shown as bright spots at positive and dark holes at negative bias voltages.

### Functionalizing the STM tip with surface oxygen

To obtain the subtle details of the lattice and orbital geometry of the Ir-O bonds, we functionalize the metallic STM tip by transferring surface oxygen atoms to the forefront of the STM tip (the details of the tip preparation can be found in Supplementary Figure 4). When imaging the $Na_2IrO_3$ surface with O-decorated tips, we observe ultrahigh spatial resolution imaging initially, as shown in Figure 3A. The zoomed image [Figure 3B] indicates that each Na atom is imaged as a protrusion with a hexagonal outline instead of a circle. The hexagonal outline comprises six dark hole terminals and six less-dark side connections. The distance between adjacent dark holes is 3.1 Å, very close to the Ir-O-Ir bond length (3.17 Å) [Supplementary Figure 3], implying that the observed hexagonal dark outlines are the Ir-O-Ir bonds. Further approaching the tip to the surface leads to an even sharper orbital width [Figure 3C], suggesting an extremely high-resolution of the imaging by the O-decorated tip and the localization of Ir 5*d* orbitals. Such resolution enhancement with reduced tip-surface distances can be induced by the movement of oxygen atoms on the apex of the metal tip, resembling the chemical bond imaging by CO-decorated AFM tip[48,49], where the CO molecule can be dragged back and forth during the scanning.

### Visualization of the anisotropic Ir-O-Ir spin lattices

Surprisingly, the functionality of such an O-decorated tip is not limited to obtaining the ultrahigh spatial resolution. It also allows us to visualize the Ir-O-Ir bonds and the subtle difference between the orbitals

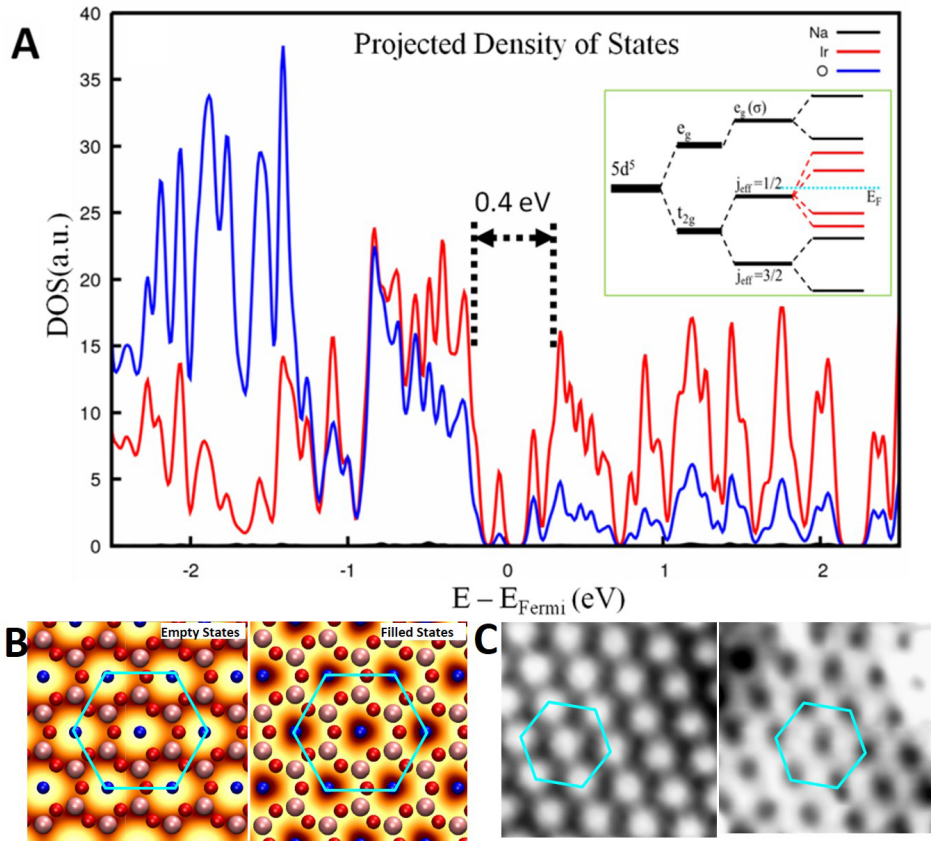


**Figure 2.** DFT calculated PDOS and the simulated STM images of the pristine $Na_2IrO_3$ surface. (A) The calculated PDOS of the top Na layer (red, 1st-Na), the second O layer (black, 2nd-O) and the Ir (blue, 3rd-Ir) in the third layer, respectively. The inset shows the schematic crystal field splitting of the 5*d* level in the half-filling case with $J_{eff}$ = 1/2. (B) The simulated empty (+2.0 eV) and filled (-2.0 eV) state STM images using an Ir(111) tip. The superimposed Na, O and Ir atoms are represented with blue, red and pink balls, respectively. (C) Experimental STM images acquired at +2.0 V (left) and -2.0 V (right), respectively. The unit cells of the honeycomb lattice of the $Na_2IrO_3$ surface are indicated with cyan hexagons.

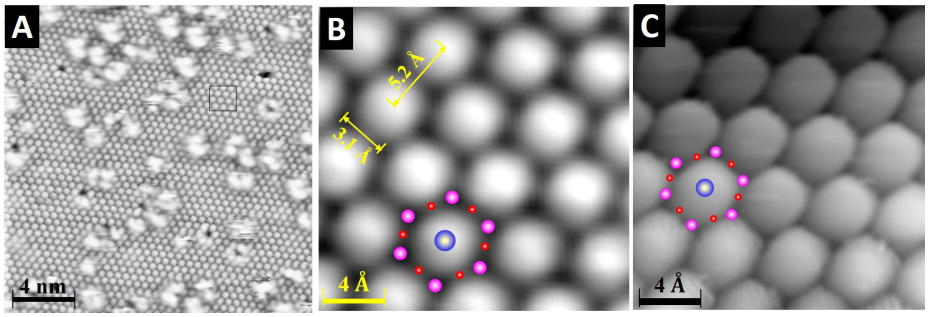


**Figure 3.** Enhanced spatial resolution by an O-decorated STM tip. (A) STM image of the $Na_2IrO_3$ surface taken with an O-decorated tip ($V_b$ = -1.8 V, $I_t$ = 20 pA, image size: 20 × 20 $nm^2$). (B) Zoomed STM image from the region marked by black rectangle in (A). The superimposed Na, O and Ir atoms are represented with blue, red and pink balls, respectively. By measuring the line profiles, the distance between the nearest-neighboring Na atoms is 5.2 Å, and the length of Ir-O-Ir bonds is 3.1 Å. (C) Ultra-highly resolved image for the same area taken with $V_b$ = -1.6 V.

directly. The $Na_2IrO_3$ lattice is known to be a near-perfect hexagonal, isotropic lattice. This fact has been evidenced by both our DFT optimized surface structure [Figure 3], the STM topographic image with

normal Ir tip [Figure 1A] and the X-ray diffraction experiments[10,14], giving almost identical Ir-O-Ir lengths and bonding angles. However, at the surface regions far from the oxygen vacancies, the imaging with O-decorated tips leads to an unexpected anisotropic, zigzag pattern at a narrow energy window (-1.6 to -1.2 eV), as shown in Supplementary Figure 5. Figure 4A presents the coexistence of the hexagonal Na lattice and the zigzag patterns measured at -1.6 V, thus rule out the influence of the tip shape effect. The zoomed image [Figure 4B] indicates that the dark holes are the Na atoms, and the zigzag pattern corresponds to the Ir-O-Ir bonds. To reveal the nature of the anisotropic Ir-O-Ir lattice, we measured the height profiles [Figure 4C] along X, Y and Z directions between the nearest neighbor Ir atoms, respectively. Interestingly, the profile along the Z direction is prominently different from that along the X and Y directions. Such anisotropy cannot be simply attributed to the structural difference.

It is well known that the charges, orbitals and spins are strongly correlated and entangled in TMO materials. The observed anisotropic Ir-O-Ir orbitals may stem from either novel charge-ordered states or spin distribution due to the strong spin-orbit interactions. Since no novel charge-ordered states were proposed or observed in previous theoretical/experimental works, we attribute such anisotropic orbitals to the spin distribution on this surface. The spin-polarized distributions of electronic states of the $Na_2IrO_3$ surface are shown in Figure 5A. Considering that the electronic states on the Na atoms are negligibly small, the top layer Na atoms are removed for better visualization [Figure 5A]. As demonstrated, the spin-up states (green contours) are mostly localized on the Ir and O atoms, while the spin-down states (yellow contours) are distributed at the Ir-O bonds. The key information given here is that the distribution of spin-up and spin-down states on this surface is intrinsically separated in the real space. Figure 5B shows the energy dependence of spin-polarized DOS (sDOS) for the spin-up and spin-down states (left panel) and the difference between the DOS of the two states (right panel) on the top layer of Ir and O atoms. It is clearly seen that the occupied spin-down states are more profound than the spin-up states in the energy ranges of -0.5 to 0.0 eV and -1.8 to -1.4 eV, while the spin-up states are more prominent in the energy ranges of -1.4 to -0.5 eV. Such characteristics suggest that the spin-up and spin-down states on this surface can be discriminated at different energy scales. As shown in Figure 4B and C, the main difference between the line profiles along the X, Y and Z directions is the contrast of the central O atom of Ir-O-Ir bonds. Along the Z direction, the contrast of the central O atom is much weaker than that along the X and Y directions, suggesting a different spin-up state intensity localized at O atoms. In order to visualize the surface spin density, the predominant condition is that the states of the STM tip should be spin polarized. We constructed an O-decorated Ir tip from the DFT calculations, as shown in Figure 5C. The details of the tip model and the computational methods are described in the Supplementary Materials. Figure 5D shows that the sDOS of the O-functionalized tip apex exhibits spin polarization near the Fermi level. As a result, the surface spin texture mostly localized at Ir-O-Ir bonds can be resolved by the oxygen-functionalized tip. It is worth noting that the above calculations of surface sDOS did not consider a specific spin structure.

Schematically, the zigzag pattern and the anisotropy of the Ir-O-Ir bonds could originate from the antiferromagnetic spin ordering of $J_{\text{eff}} = 1/2$ electrons. Zigzag-type magnetic order was first proposed[3,15,17] and confirmed experimentally[4,14,50] as the most likely ground state for $Na_2IrO_3$. Magnetic and heat-capacity measurements[10] also suggest that short-range magnetic order develops within the $NaIr_2O_6$ layers in $Na_2IrO_3$ at a temperature well above $T_N$. In the scheme of zigzag-type magnetic order, each Ir atom has two nearest-neighbor Ir atoms with parallel $J_{\text{eff}} = 1/2$ spin and one Ir atom with antiparallel spin. The hopping terms between extended Ir 5*d* orbitals include an indirect hopping through the oxygen 2*p* orbital ($t_{\text{pd}}$), and two kinds of direct hopping between neighboring Ir atoms ($t_{\text{dd1}}$ and $t_{\text{dd2}}$)[8]. When an electron hops from Ir atom *i* to atom *j*, the effective transfer integral is given by $t_{ij} = t\langle x_i|x_j\rangle = t\cos(\theta_{ij}/2)$, where $\theta_{ij}$ is the angle between the two spins. Therefore, $|t_{ij}|$ is the maximum for parallel spins and is zero for antiparallel spins. As shown in

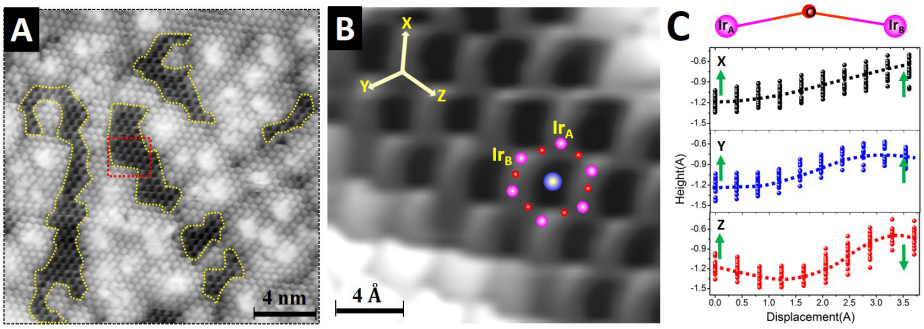


**Figure 4.** The visualization of the anisotropic Ir-O-Ir lattices at negative biases. (A) The STM image of the $Na_2IrO_3$ surface taken with an O-decorated tip. The regions highlighted by yellow curves exhibit the zigzag pattern ($V_b$ = -1.6 V, $I_t$ = 20 pA, image size: 20 × 20 $nm^2$). (B) Highly resolved STM image zoomed from the region marked with a red rectangle in (A). The superimposed Na, O and Ir atoms are represented with blue, red and pink balls, respectively. Ir atoms show differences in contrast, which we label as $Ir_A$ and $Ir_B$, respectively. (C) Height profiles of the $Ir_A$-O-$Ir_B$ bonds along the nearest-neighbor directions of X, Y and Z.

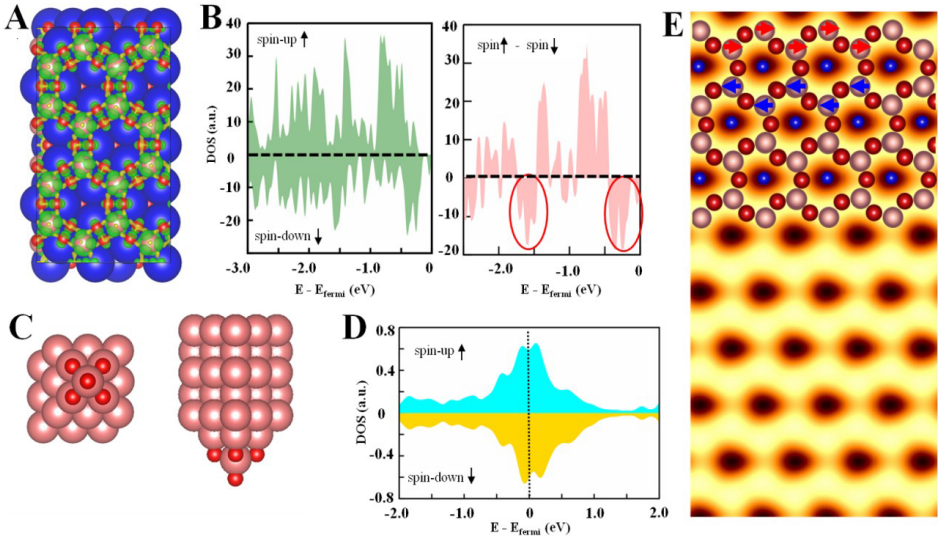


**Figure 5.** (A) The spin-polarized charge density distribution of a $Na_2IrO_3$ surface. The top layer of Na is removed for better visualization. The spin-up states (localized at the Ir and O atoms) and the spin-down states (localized in between the Ir and O atoms) are represented with green and yellow contours, respectively. The Na, Ir and O atoms are shown as blue, pink and red circles, respectively. (B) The difference of spin-up and spin-down states of the top Ir and O layers. (C) The top (left) and the side view (right) of the oxygen-decorated Ir tip model. (D) The spin-polarized DOS of the oxygen atom at the apex of the Ir-O tip. (E) Spin-polarized STM simulation imaged with the O-decorated Ir(111) tip ($V_b$ = -1.6 V).

Figure 4C, the spins are antiparallel along the Z direction and are parallel along the X and Y directions, leading to the hopping term along the Z direction being smaller than that along the X and Y directions. Thus, the observed zigzag pattern in Figure 4B reflects the short-range zigzag spin order and the strong spin-orbit interactions that lock the lattice and magnetic moments. By considering the spin polarization of the oxygen-functionalized STM tip and the zigzag AFM spin ordering of the surface, our simulated STM image [Figure 5E] indeed leads to a zigzag pattern of Ir-O-Ir lattice, agreeing with the experimental observation [Figure 4B].

## CONCLUSIONS

In summary, a 420 meV Mott insulating gap is identified on the surface of $Na_2IrO_3$ crystal. Ultra-high resolution STM images are achieved by functionalizing the STM tip with surface oxygen atoms. A zigzag-like topology of the Ir-O-Ir lattices is directly visualized, and the anisotropic Ir-O bonds along different lattice orientations are revealed within a narrow energy window. The direct observation of a zigzag Ir-O-Ir lattice at 77 K dictates the zigzag magnetic order below $T_N \approx 15$ K because of the strong spin-orbit interactions. Our results provide a novel approach to investigate the interactions between the lattices, charge and spin degrees of freedom of strongly correlated oxides.

## DECLARATIONS

### Authors' contributions

Conceived the idea: Pan M
Designed the STM work: Zhang X, Zhang Z, Shao Z, Sun H, Li S, Ding H, Gao J, Zhu W, Pan M
Conducted theoretical calculations: Palotás K, Lin H
Performed materials fabrication: Terzic J, Gang Cao
Wrote the paper with help from others: Gao J, Pan M

### Availability of data and materials

All data needed to evaluate the conclusions in the paper are present in the paper and/or the Supplementary Materials. Additional data related to this paper may be requested from the authors.

### Financial support and sponsorship

This work was supported by the National Major State Basic Research Development Program (2017YFA0205000) and the National Science Foundation of China (21872099, 21622306, 21771134, 11574095 and 12104004). Palotás K acknowledges funding from NRDIO Hungary (FK124100).

### Conflicts of interest

All authors declared that there are no conflicts of interest.

### Ethical approval and consent to participate

Not applicable.

### Consent for publication

Not applicable.



## REFERENCES

1. Chaloupka J, Jackeli G, Khaliullin G. Kitaev-Heisenberg model on a honeycomb lattice: possible exotic phases in iridium oxides $A_2IrO_3$. *Phys Rev Lett* 2010;105:027204. DOI PubMed
2. Choi SK, Coldea R, Kolmogorov AN, et al. Spin waves and revised crystal structure of honeycomb iridate $Na_2IrO_3$. *Phys Rev Lett* 2012;108:127204. DOI
3. Chaloupka J, Jackeli G, Khaliullin G. Zigzag magnetic order in the iridium oxide $Na_2IrO_3$. *Phys Rev Lett* 2013;110:097204. DOI PubMed
4. Liu X, Berlijn T, Yin W, et al. Long-range magnetic ordering in $Na_2IrO_3$. *Phys Rev B* 2011;83:220403. DOI
5. Hu K, Wang F, Feng J. First-principles study of the magnetic structure of $Na_2IrO_3$. *Phys Rev Lett* 2015;115:167204. DOI PubMed
6. Takagi H, Takayama T, Jackeli G, Khaliullin G, Nagler SE. Concept and realization of Kitaev quantum spin liquids. *Nat Rev Phys* 2019;1:264-80. DOI
7. Shitade A, Katsura H, Kunes J, Qi XL, Zhang SC, Nagaosa N. Quantum spin Hall effect in a transition metal oxide $Na_2IrO_3$. *Phys Rev*

*Lett* 2009;102:256403. DOI
8. Kim CH, Kim HS, Jeong H, Jin H, Yu J. Topological quantum phase transition in 5d transition metal oxide $Na_2IrO_3$. *Phys Rev Lett* 2012;108:106401. DOI
9. Sohn CH, Kim H, Qi TF, et al. Mixing between $J_{eff}$= 1/2 and 3/2 orbitals in $Na_2IrO_3$: a spectroscopic and density functional calculation study. *Phys Rev B* 2013;88:085125. DOI
10. Singh Y, Gegenwart P. Antiferromagnetic Mott insulating state in single crystals of the honeycomb lattice material $Na_2IrO_3$. *Phys Rev B* 2010;82:064412. DOI
11. Comin R, Levy G, Ludbrook B, et al. $Na_2IrO_3$ as a novel relativistic Mott insulator with a 340-meV gap. *Phys Rev Lett* 2012;109:266406. DOI
12. Gretarsson H, Clancy JP, Liu X, et al. Crystal-field splitting and correlation effect on the electronic structure of $A_2IrO_3$. *Phys Rev Lett* 2013;110:076402. DOI
13. Kim HJ, Lee JH, Cho JH. Antiferromagnetic slater insulator phase of $Na_2IrO_3$. *Sci Rep* 2014;4:5253. DOI PubMed PMC
14. Ye F, Chi S, Cao H, et al. Direct evidence of a zigzag spin-chain structure in the honeycomb lattice: a neutron and X-ray diffraction investigation of single-crystal $Na_2IrO_3$. *Phys Rev B* 2012;85:180403. DOI
15. Kimchi I, You Y. Kitaev-Heisenberg-$J_2$-$J_3$ model for the iridates $A_2IrO_3$. *Phys Rev B* 2011;84:180407. DOI
16. Bhattacharjee S, Lee S, Kim YB. Spin-orbital locking, emergent pseudo-spin and magnetic order in honeycomb lattice iridates. *New J Phys* 2012;14:073015. DOI
17. Rau JG, Lee EK, Kee HY. Generic spin model for the honeycomb iridates beyond the Kitaev limit. *Phys Rev Lett* 2014;112:077204. DOI PubMed
18. Baek SH, Do SH, Choi KY, et al. Evidence for a field-induced quantum spin liquid in α-$RuCl_3$. *Phys Rev Lett* 2017;119:037201. DOI
19. Bastien G, Garbarino G, Yadav R, et al. Pressure-induced dimerization and valence bond crystal formation in the Kitaev-Heisenberg magnet α-$RuCl_3$. *Phys Rev B* 2018;97:037201. DOI
20. Hu K, Zhou Z, Wei Y, Li C, Feng J. Bond ordering and phase transitions in $Na_2IrO_3$ under high pressure. *Phys Rev B* 2018;98:100103. DOI
21. Simutis G, Barbero N, Rolfs K, et al. Chemical and hydrostatic-pressure effects on the Kitaev honeycomb material $Na_2IrO_3$. *Phys Rev B* 2018;98:104421. DOI
22. Xi X, Bo X, Xu XS, et al. Honeycomb lattice $Na_2IrO_3$ at high pressures: a robust spin-orbit Mott insulator. *Phys Rev B* 2018;98:125117. DOI
23. Jiang H, Gu Z, Qi X, Trebst S. Possible proximity of the Mott insulating iridate $Na_2IrO_3$ to a topological phase: phase diagram of the Heisenberg-Kitaev model in a magnetic field. *Phys Rev B* 2011;83:245104. DOI
24. Reuther J, Thomale R, Trebst S. Finite-temperature phase diagram of the Heisenberg-Kitaev model. *Phys Rev B* 2011;84:100406. DOI
25. Yamaji Y, Nomura Y, Kurita M, Arita R, Imada M. First-principles study of the honeycomb-lattice iridates $Na_2IrO_3$ in the presence of strong spin-orbit interaction and electron correlations. *Phys Rev Lett* 2014;113:107201. DOI PubMed
26. Rousochatzakis I, Reuther J, Thomale R, Rachel S, Perkins N. Phase diagram and quantum order by disorder in the Kitaev K1-K2 honeycomb magnet. *Phys Rev X* 2015;5:041035. DOI
27. Fischer Ø, Kugler M, Maggio-aprile I, Berthod C, Renner C. Scanning tunneling spectroscopy of high-temperature superconductors. *Rev Mod Phys* 2007;79:353-419. DOI
28. Dziuba T, Pietsch I, Stark M, Traeger GA, Gegenwart P, Wenderoth M. Surface conductivity of the honeycomb spin-orbit mott insulator $Na_2IrO_3$. *Phys Status Solidi B* 2021;258:2000421. DOI
29. Wiesendanger R, Güntherodt H, Güntherodt G, Gambino RJ, Ruf R. Observation of vacuum tunneling of spin-polarized electrons with the scanning tunneling microscope. *Phys Rev Lett* 1990;65:247-50. DOI PubMed
30. Wiesendanger R, Bürgler D, Tarrach G, et al. Vacuum tunneling of spin-polarized electrons detected by scanning tunneling microscopy. *J Vac Sci Technol B* 1991;9:519-24. DOI
31. Oka H, Brovko OO, Corbetta M, Stepanyuk VS, Sander D, Kirschner J. Spin-polarized quantum confinement in nanostructures: scanning tunneling microscopy. *Rev Mod Phys* 2014;86:1127-68. DOI
32. Pratzer M, Elmers HJ, Bode M, Pietzsch O, Kubetzka A, Wiesendanger R. Atomic-scale magnetic domain walls in quasi-one-dimensional Fe nanostripes. *Phys Rev Lett* 2001;87:127201. DOI PubMed
33. Kubetzka A, Bode M, Pietzsch O, Wiesendanger R. Spin-polarized scanning tunneling microscopy with antiferromagnetic probe tips. *Phys Rev Lett* 2002;88:057201. DOI PubMed
34. Wachowiak A, Wiebe J, Bode M, Pietzsch O, Morgenstern M, Wiesendanger R. Direct observation of internal spin structure of magnetic vortex cores. *Science* 2002;298:577-80. DOI PubMed
35. Bode M, Heide M, von Bergmann K, et al. Chiral magnetic order at surfaces driven by inversion asymmetry. *Nature* 2007;447:190-3. DOI
36. Horcas I, Fernández R, Gómez-Rodríguez JM, Colchero J, Gómez-Herrero J, Baro AM. WSXM: a software for scanning probe microscopy and a tool for nanotechnology. *Rev Sci Instrum* 2007;78:013705. DOI
37. Kresse G, Furthmüller J. Efficient iterative schemes for ab initio total-energy calculations using a plane-wave basis set. *Phys Rev B Condens Matter* 1996;54:11169-86. DOI PubMed
38. Kresse G, Joubert D. From ultrasoft pseudopotentials to the projector augmented-wave method. *Phys Rev B* 1999;59:1758-75. DOI
39. Perdew JP, Burke K, Ernzerhof M. Generalized gradient approximation made simple. *Phys Rev Lett* 1996;77:3865-8. DOI PubMed

40. Hofer WA, Foster AS, Shluger AL. Theories of scanning probe microscopes at the atomic scale. *Rev Mod Phys* 2003;75:1287-331. DOI
41. Park K, Meunier V, Pan M, Shelton W, Yu N, Plummer E. Nanoclusters of $TiO_2$ wetted with gold. *Surf Sci* 2009;603:3131-5. DOI
42. Li G, Li Q, Pan M, et al. Atomic-scale fingerprint of Mn dopant at the surface of $Sr_3(Ru_{1-x}Mn_x)_2O_7$. *Sci Rep* 2013;3:2882. DOI PubMed PMC
43. Lüpke F, Manni S, Erwin SC, Mazin II, Gegenwart P, Wenderoth M. Highly unconventional surface reconstruction of $Na_2IrO_3$ with persistent energy gap. *Phys Rev B* 2015;91:041405. DOI
44. Kim BJ, Jin H, Moon SJ, et al. Novel $J_{eff}$ = 1/2 Mott state induced by relativistic spin-orbit coupling in $Sr_2IrO_4$. *Phys Rev Lett* 2008;101:076402. DOI
45. Kim BJ, Ohsumi H, Komesu T, et al. Phase-sensitive observation of a spin-orbital Mott state in $Sr_2IrO_4$. *Science* 2009;323:1329-32. DOI
46. Calder S, Garlea VO, McMorrow DF, et al. Magnetically driven metal-insulator transition in $NaOsO_3$. *Phys Rev Lett* 2012;108:257209. DOI
47. Slater JC. Magnetic effects and the hartree-fock equation. *Phys Rev* 1951;82:538-41. DOI
48. Gross L, Mohn F, Moll N, Liljeroth P, Meyer G. The chemical structure of a molecule resolved by atomic force microscopy. *Science* 2009;325:1110-4. DOI PubMed
49. Zhang J, Chen P, Yuan B, Ji W, Cheng Z, Qiu X. Real-space identification of intermolecular bonding with atomic force microscopy. *Science* 2013;342:611-4. DOI
50. Hwan Chun S, Kim J, Kim J, et al. Direct evidence for dominant bond-directional interactions in a honeycomb lattice iridate $Na_2IrO_3$. *Nat Phys* 2015;11:462-6. DOI